Finite-Element Analysis of Cylindrical Panels with Random Initial Imperfections

Vissarion Papadopoulos[1] and Manolis Papadrakakis[2]

Abstract: Stochastic finite-element analysis of shells is performed using the spectral representation method for the description of the random fields in conjunction with the local average method for the formulation of the stochastic stiffness matrix of the elements. A stochastic formulation of the nonlinear triangular composites facet triangular shell element is implemented for the stability analysis of cylindrical panels with random initial imperfections. The imperfections are described as a two-dimensional univariate homogeneous stochastic field. The elastic modulus and the shell thickness are also described as two-dimensional uni-variate homogeneous stochastic fields. The variability of the limit load of the cylindrical panel is then computed using the Monte Carlo simulation. Useful conclusions for the buckling behavior of cylindrical panels with random initial imperfections are derived from the numerical tests presented in this paper. These tests also demonstrate the applicability of the proposed methodology in realistic problems.

DOI: 10.1061/(ASCE)0733-9399(2004)130:8(867)

CE Database subject headings: Finite elements; Imperfection; Stochastic processes; Panels.

Introduction

The analysis of imperfection sensitive shells has attracted the attention of many researchers in the past decades due to the crucial role that imperfections play in the buckling and postbuckling behavior of shell structures. Even though these research efforts resulted in achieving predictions close to the experimental results, it was soon realized that the wide scatter in measured buckling loads of shell structures could only be approximated through modeling with the introduction of randomness in imperfect geometries. This can only be achieved in conjunction with recent developments in stochastic analysis of structures and in the nonlinear analysis of shells. Despite these new developments, the accurate prediction of the load carrying capacity of imperfect shells is still an open question in the related literature (Chryssanthopoulos and Poggi 1995; Deml and Wunderlich 1997; Albertin and Wunderlich 2000; Schenk et al. 2000). The variability of initial imperfections, which occur during the manufacturing and construction stages together with their pronounced influence on the load carrying capacity of shells have been found to be responsible for the large scatter of results observed in experimental tests. In addition to the initial geometric imperfections, the effect of thickness variation, the modulus of elasticity and the boundary conditions have also been proved responsible for the reduction as well as the scatter of the buckling load of structures (Koiter et al. 1994; Elishakoff et al. 1996; Li et al. 1997; Albertin and Wunderlich 2000). However, in a number of studies these influencing parameters have not been treated as stochastic variables in a rational manner and for this reason recent research activity is concentrated on the development of finite-element codes in a stochastic setting, incorporating uncertain imperfections, elastic moduli, boundary conditions, thickness variation, and loading conditions (Schenk et al. 2000).

In the present paper a methodology is presented for the stochastic nonlinear finite-element analysis of shells in the presence of random initial imperfections. The formulation is based on the stochastic description of the initial imperfections. The term ''imperfections'' is used in a general sense meaning not only geometric imperfections but also the variability of material properties as well as thickness of the shell. These imperfections are described as two-dimensional univariate homogeneous stochastic fields (2-D-1V) using the spectral representation method (Shinozuka and Deodatis 1996) and are incorporated in a nonlinear stochastic finite-element formulation of the triangular composites (TRIC) shell element using the local average method for the derivation of the stochastic stiffness matrix (Argyris et al. 2002). The variability of the limit loads is obtained with the Monte Carlo simulation technique (MCS).

The nonlinear formulation of the TRIC shell element is based on the natural mode method. The blending of the natural mode method with a path following strategy presents many advantages compared to classical formulations, i.e., analytic and elegant expressions for all element matrices; a series of vector and matrice multiplications that can be easily optimized for maximum computational speed; material generality; accurate location of bifurcation limit and displacement points; computational efficiency and economy (Argyris et al. 1998, 2000). This formulation is therefore considered a robust platform for the accurate prediction of the buckling and postbuckling behavior of imperfect shells.

The numerical results presented in this paper demonstrate the applicability as well as the efficiency of the proposed methodology in realistic problems. Useful conclusions are derived for the buckling behavior of cylindrical panels. More specifically, the influence of the magnitude as well as the shape, controlled by the

[1]Institute of Structural Analysis and Seismic Research, National Technical Univ., Athens 15780, Greece. E-mail: vpapado@central.ntua.gr

[2]Institute of Structural Analysis and Seismic Research, National Technical Univ., Athens 15780, Greece. E-mail: mpapadra@central.ntua.gr

Note. Associate Editor: Gerhart I. Schueller. Discussion open until January 1, 2005. Separate discussions must be submitted for individual papers. To extend the closing date by one month, a written request must be filed with the ASCE Managing Editor. The manuscript for this paper was submitted for review and possible publication on February 20, 2002; approved on June 2, 2003. This paper is part of the ***Journal of Engineering Mechanics***, Vol. 130, No. 8, August 1, 2004. ©ASCE, ISSN 0733-9399/2004/8-867–876/$18.00.

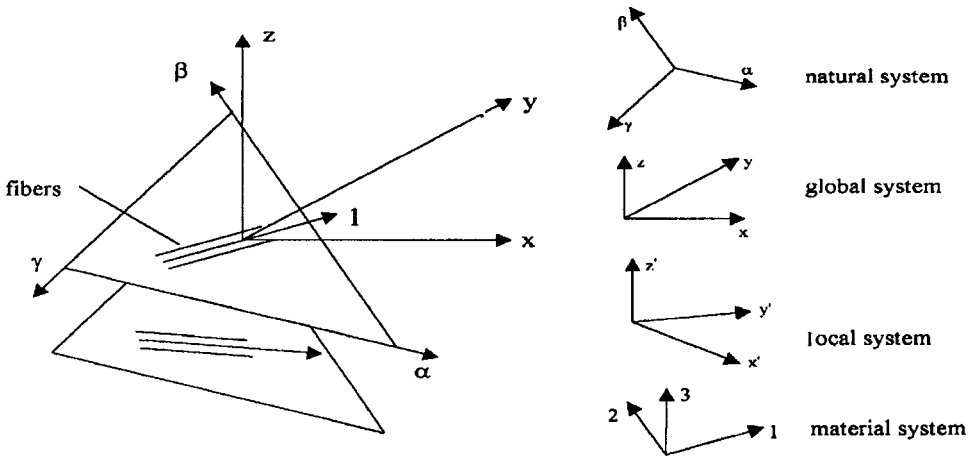

Fig. 1. The multilayer triangular composites (TRIC) element; coordinate systems

correlation length, of the initial geometric imperfections is investigated independently and in conjunction with the variability of the elastic modulus as well as the thickness of the structure.

Finite-Element Formulation

An attempt to devise an efficient and robust shell finite element led Argyris and co-workers to the derivation of the TRIC shell element. The formulation is based on the natural mode method. TRIC is a shear-deformable facet shell element suitable for linear and nonlinear analysis of thin and moderately thick isotropic as well as composite plate and shell structures, while due to its natural formulation it does not suffer from the various locking phenomena. In this work TRIC is used in the context of nonlinear static analysis of isotropic shells but laminate anisotropic shells can be analyzed in a similar fashion since the proposed methodology doesn't depend on the formulation of the finite-element problem. The TRIC shell element is considered as reliable, accurate, and cost effective as has been shown in a number of studies published over the last five years. For the sake of completeness a brief description of the TRIC shell element is given in this section. Extensive reports on the formulation of TRIC may be found in Argyris et al. (1997, 1998, 2000).

The TRIC shell element. The element has 18 degrees of freedom (6 per node) and hence 12 natural straining modes (Figs. 1 and 2). Three natural axial strains γ_t and natural transverse shear strains γ_s are measured parallel to the edges of the triangle. The corresponding natural stresses σ_c and the natural transverse shear stresses σ_s are obtained following a series of calculations for each layer r:

$$\begin{Bmatrix} \sigma_c \\ \sigma_s \end{Bmatrix}_r = \begin{bmatrix} \kappa_{ct} & \cdot \\ \cdot & \chi_s \end{bmatrix}_r \begin{Bmatrix} \gamma_t \\ \gamma_s \end{Bmatrix}_r \tag{1a}$$

where the total strains γ_t and the symmetric bending modes, shown in Fig. 2(a), are connected via

$$\gamma_{t\alpha} = \gamma_{t\alpha}^0 + z' \frac{\psi_{S\alpha}}{l_\alpha}$$

$$\gamma_{t\beta} = \gamma_{t\beta}^0 + z' \frac{\psi_{S\beta}}{l_\beta} \tag{1b}$$

$$\gamma_{t\gamma} = \gamma_{t\gamma}^0 + z' \frac{\psi_{S\gamma}}{l_\gamma}$$

where $l_i\,(i=\alpha,\beta,\gamma)$=length of side i and z'=distance from the middle surface along z' axis of the element. The natural transverse strains γ_s are shown in Fig. 2(b).

Matrices κ_{ct} and χ_s are constitutive matrices. The stiffness is contributed by deformations only and not by the associated rigid body motions. The natural stiffness matrix can be produced from the statement of variation of the strain energy with respect to the natural coordinates:

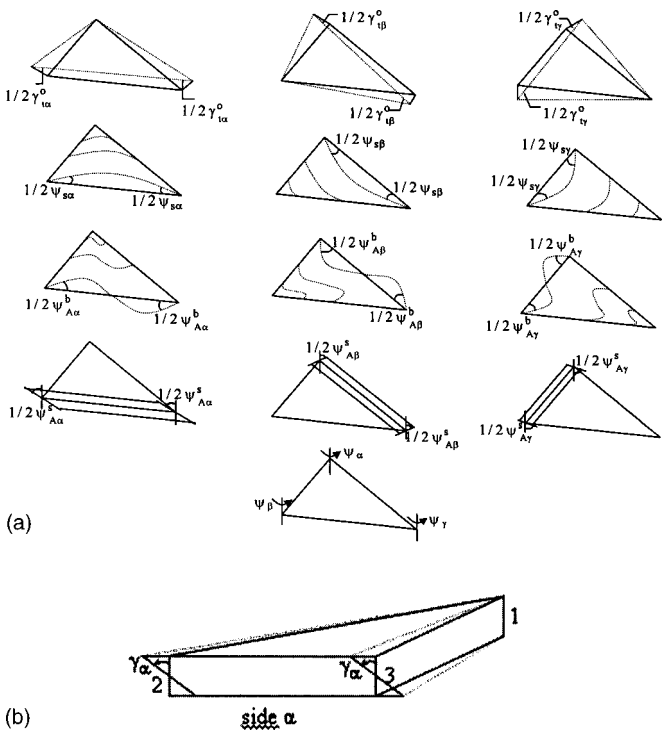

Fig. 2. (a) The 12 natural straining modes (γ_t^0: natural axial strains in the middle surface, ψ_S: symmetric bending modes, ψ_A^b: antisymmetric bending modes, ψ_A^S antisymmetric shearing modes, ψ: drilling degrees of freedom). (b) Total natural transverse shear for side *a*.

$$\delta U=\int_V \sigma_c^T \delta\gamma_t dV \xrightarrow{(1)} \delta U=\int_V \gamma_t^T \kappa_{ct} \delta\gamma_t dV \Bigg\} \quad \gamma_t=\alpha_N \rho_N$$

$$\rightarrow \delta U=\rho_N^T \left[\int_V \alpha_N^T \kappa_{ct} \alpha_N dV\right] d\rho_N \tag{2}$$

where ρ_N=vector of the 12 natural straining modes depicted in Fig. 2(a). Transformations are subsequently initiated in order to obtain the natural matrix first to the local and then to the global coordinate system:

$$\delta U=\rho^T \underbrace{\left[\underbrace{\bar{\alpha}_N^T \underbrace{\left[\underbrace{\int_V \alpha_N^T \kappa_{ct} \alpha_N dV}_{\text{stiffness natural coord. (12x12)}}\right]}_{\text{stiffness local coord. (18x18)}} \bar{\alpha}_N}_{\text{stiffness global coord. (18x18)}} T_{06}\right]}_{} \rho, \text{ where } \rho=\bar{\alpha}_N \rho_N \tag{3}$$

$$\underset{(3\times 3)}{\bar{k}_{GR}}=\begin{bmatrix} \frac{P_\alpha y_\alpha^2}{l_\alpha^2}+\frac{P_\beta y_\beta^2}{l_\beta^2}+\frac{P_\gamma y_\gamma^2}{l_\gamma^2} & -\left(\frac{P_\alpha x_\alpha y_\alpha}{l_\alpha^2}+\frac{P_\beta x_\beta y_\beta^2}{l_\beta^2}+\frac{P_\gamma x_\gamma y_\gamma^2}{l_\gamma^2}\right) & 0 \\ -\left(\frac{P_\alpha x_\alpha y_\alpha}{l_\alpha^2}+\frac{P_\beta x_\beta y_\beta^2}{l_\beta^2}+\frac{P_\gamma x_\gamma y_\gamma^2}{l_\gamma^2}\right) & \frac{P_\alpha x_\alpha^2}{l_\alpha^2}+\frac{P_\beta x_\beta^2}{l_\beta^2}+\frac{P_\gamma x_\gamma^2}{l_\gamma^2} & 0 \\ 0 & 0 & P_\alpha+P_\beta+P_\gamma \end{bmatrix} \tag{4}$$

where P_α, P_β, P_γ=middle plane axial natural forces and

$$x_\alpha=l_\alpha c_{\alpha x}=x_3'-x_2', \quad x_\beta=l_\beta c_{\beta x}=x_1'-x_3'$$

$$x_\gamma=l_\gamma c_{\gamma x}=x_2'-x_1'$$

$$y_\alpha=l_\alpha c_{\alpha x}=y_3'-y_2', \quad y_\beta=l_\beta c_{\beta x}=y_1'-y_3'$$

$$y_\gamma=l_\gamma c_{\gamma x}=y_2'-y_1'$$

are geometric expressions with x_1', y_1', x_2', y_2', x_3', y_3' being the x', y' coordinates of the three vertices of the facet triangle in the local Cartesian system. A transformation of $\bar{k}_{GR}$ to the local coordinate system follows from

$$\underset{(18\times 18)}{\bar{k}_G}=\underset{(18\times 3)(3\times 3)(3\times 18)}{\bar{\alpha}_{0R}^t \bar{k}_{GR} \bar{\alpha}_{0R}} \tag{5a}$$

where $\bar{\alpha}_{0R}$=transformation matrix relating the natural rigid-body rotations ρ_0^2 to the Cartesian nodal displacements and rotations $\bar{\rho}$,

$$\rho_0^2=\bar{\alpha}_{0R}\bar{\rho} \tag{5b}$$

$\bar{k}_G$=so-called simplified geometric stiffness with respect to axes $x'y'z'$. The term simplified refers to the fact that only the middle plane axial natural forces P_α, P_β, P_γ are included in $\bar{k}_G$ which fully represent the prestress state within the material. Once the simplified geometric stiffness is formed it may transformed to the global coordinate system.

As mentioned before, nearly all geometric stiffness arises from the rigid-body movements of the element. However, in buckling phenomena quite often the membrane forces are relatively large and in this case it may be worth considering an additional approximate natural geometric stiffness arising from the coupling between the axial forces and the symmetric bending mode (stiffening or softening effect). This natural geometric stiffness comprises the following diagonal matrix:

$$k_{NG}=\left[0 \;\; 0 \;\; 0 \;\; \frac{P_\alpha l_\alpha}{12} \;\; \frac{P_\alpha l_\alpha}{20} \;\; \frac{P_\beta l_\beta}{12} \;\; \frac{P_\beta l_\beta}{20} \;\; \frac{P_\gamma l_\gamma}{12} \;\; \frac{P_\gamma l_\gamma}{20} \;\; 0 \;\; 0 \;\; 0\right] \tag{6}$$

A derivation of this expression can be found in Argyris et al. (1998). The natural geometric stiffness is then transformed first to local and ultimately to the global coordinates.

Description of Initial Imperfect Geometry

The imperfect geometry of shell structures can be accurately represented as a two-dimensional uni-variate homogeneous Gaussian stochastic field. The assumption of homogeneity, although in general violated in the case of initial geometric imperfections, is adopted in this study and elsewhere (Schenk et al. 2000) in the case of cylindrical panels, for reasons of simplicity and due to the fact that there are no experimental data available for this type of cylindrical panels. However, this method can be easily extended

to cover non-Gaussian and nonhomogeneous stochastic fields (Popescu et al. 1998; Schenk et al. 2000).

The radius of the structure is assumed to be a 2-D-1V homogeneous stochastic field with respect to the perfect geometry

$$r(x,y)=r_0+f_1(x,y)h \tag{7}$$

where r_0=radius of the perfect geometry; $f_1(x,y)$=zero mean Gaussian homogeneous stochastic field; and h=height at the apex of the cylindrical panel. In the present paper the amplitude of the imperfections, which is controlled by the standard deviation of the stochastic field, is correlated to the height at the apex of the cylindrical panel since this parameter is related to the sensitivity of the buckling behavior of the cylindrical panel to initial geometric imperfections. The coordinates *x, y* are the global Cartesian coordinates of the unfolded panel.

Moreover, the shape of the imperfections is controlled by the correlation lengths of the stochastic field $f_1(x,y)$ in directions *x* and *y*, respectively. These correlation lengths are usually derived from experimental data and play a significant role on the buckling behavior of shells. Since no experimental data are available for this type of problem, a parametric study is performed in the present study, with respect to the correlation lengths of the stochastic field in both *x, y* directions. The outcome of this parametric study is the evaluation of the ''worst'' imperfection mode of the shell which leads to the estimation of the lower bound of the buckling load of the shell. This information is most valuable for the safe design of shells against buckling [Deml and Wunderlich 1997].

Stochastic Stiffness Matrix

The modulus of elasticity as well as the thickness of the structure are also considered in the present study as ''imperfections,'' due to their spatial variability. Therefore, these parameters are also described by two independent 2-D-1V homogeneous stochastic fields

$$E(x,y)=E_0[1+f_2(x,y)] \tag{8}$$

$$t(x,y)=t_0[1+f_3(x,y)] \tag{9}$$

where E_0=mean value of the elastic modulus; t_0=mean thickness of the structure; and $f_2(x,y)$, $f_3(x,y)$=two zero mean Gaussian homogeneous stochastic fields corresponding to the variability of the modulus of elasticity and the thickness of the shell, respectively.

The stochastic stiffness matrix of the shell element is derived using the local average method. This method was suggested by Vanmarcke (1983) and has been used extensively by many researchers in conjunction with the stochastic finite-element method. In a recent study by Argyris et al. (2002) it was shown that for the cylindrical panel used in our example with a vertical load on top, the local average method is superior to the weighted integral method in terms of simplicity and computational efficiency, while in terms of accuracy the results obtained are very close to those of the weighted integral method.

Given a stochastic field $f(x,y,z)$, the local average method provides discretized values of the field as follows:

$$f_i=\frac{1}{V_i}\int_{V_i} f(x,y,z)dV_i \tag{10}$$

where V_i=domain over which the integration has to be performed. In the case of stochastic finite elements, the domain represents the length (truss and beam elements), the area (plain stress/strain, plate, shell elements) or the volume (three-dimensional solid elements) of the *i*th element.

It is obvious that, according to this method, a single random variable per finite element is used to delineate the stochastic field since its random characteristics are represented by the local spatial average over each element. In this context the stochastic element stiffness matrix is expressed as

$$k^{(e)}=(1+\alpha^{(e)})k_0^{(e)} \tag{11}$$

where

$$\alpha^{(e)}=\frac{1}{V^{(e)}}\int_{V^{(e)}} f^{(e)}(x,y,z)dV^{(e)} \tag{12}$$

In the case where both the modulus of elasticity and the thickness are assumed to be simultaneously stochastic, the random variable $\alpha^{(e)}$ is given by

$$\alpha^{(e)}=\alpha_1^{(e)}\alpha_2^{(e)} \tag{13}$$

where $\alpha_1^{(e)}$ and $\alpha_2^{(e)}$=local averages corresponding to the stochastic fields of the modulus of elasticity and thickness, respectively.

The Spectral Representation Method

Since MCS technique is used to calculate the response variability of the stochastic structural system, it is necessary to digitally generate sample functions of the Gaussian zero-mean homogeneous stochastic fields, which describe the random parameters of the structure. In the present paper, this is done using the spectral representation method. In most cases, the spectral representation method takes advantage of the fast Fourier transform (FFT) technique in order to reduce the computational effort of the simulation. However, in cases that we need to simulate the stochastic field at nonuniformly spaced points, as in this work, the use of the series of cosines formula is necessary since the FFT technique is not applicable. For a 2-D-1V stochastic field and for a specific simulation (*i*), we have

$$f^{(i)}(x_1,x_2)=\sqrt{2}\sum_{n_1=0}^{N_1-1}\sum_{n_2=0}^{N_2-1}[A_{n_1n_2}^{(1)}\cos(\kappa_{1n_1}x_1+\kappa_{2n_2}x_2+\phi_{n_1n_2}^{(1)(i)}) + A_{n_1n_2}^{(2)}\cos(\kappa_{1n_1}x_1-\kappa_{2n_2}x_2+\phi_{n_1n_2}^{(2)(i)})] \tag{14}$$

where $\phi_{n_1n_2}^{(j)(i)}$, $j=1, 2$ represent the realization for the (*i*) simulation of the independent random phase angles uniformly distributed in the range $[0,2\pi]$. $A_{n_1n_2}^{(1)}$, $A_{n_1n_2}^{(2)}$ are defined as

$$A_{n_1n_2}^{(1)}=\sqrt{2S_{f_0f_0}(\kappa_{1n_1},\kappa_{2n_2})\Delta\kappa_1\Delta\kappa_2} \tag{15a}$$

$$A_{n_1n_2}^{(2)}=\sqrt{2S_{f_0f_0}(\kappa_{1n_1},-\kappa_{2n_2})\Delta\kappa_1\Delta\kappa_2} \tag{15b}$$

where

$$\kappa_{1n_1}=n_1\Delta\kappa_1, \quad \kappa_{2n_2}=n_2\Delta\kappa_2 \tag{16}$$

$$\Delta\kappa_1=\frac{\kappa_{1u}}{N_1}, \quad \Delta\kappa_2=\frac{\kappa_{2u}}{N_2} \tag{17}$$

$$n_1=0,1,...,N_1-1, \quad n_2=0,1,...,N_2-1 \tag{18}$$

N_j, $j=1, 2$, are the numbers of intervals in the discretization of the spectrum and κ_{ju}, $j=1, 2$, are the upper cut-off wave num-

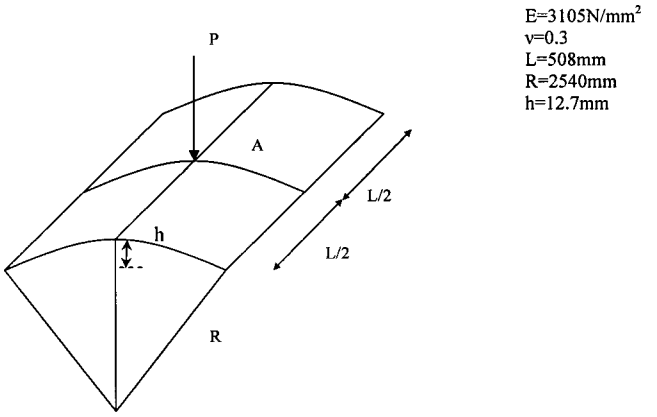

Fig. 3. Geometry, and material data of the cylindrical panel

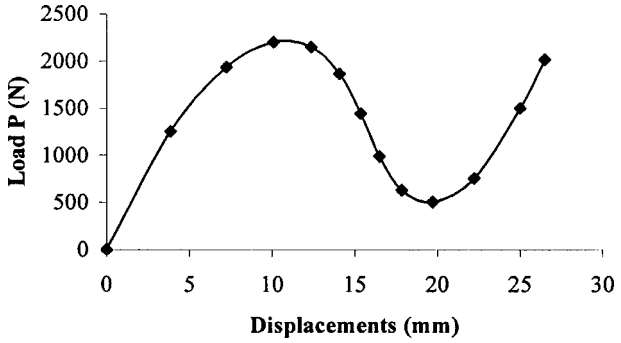

Fig. 4. Central load—displacement curve of the perfect cylindrical panel ($t=12.7$ mm)

bers which define the active region of the power spectrum $S_{f_0f_0}$ of the stochastic field. The last implies that the power spectral density function $S_{f_0f_0}(\kappa_1,\kappa_2)$, for either mathematical or physical reasons, is assumed to be zero outside the region defined by

$$-\kappa_{1u}\leqslant\kappa_1\leqslant\kappa_{1u}, \quad -\kappa_{2u}\leqslant\kappa_2\leqslant\kappa_{2u} \tag{19}$$

The two-sided power spectral density function $S_{f_0f_0}$ is assumed to correspond to an autocorrelation function of exponential type and is given by

$$S_{f_0f_0}(\kappa_1,\kappa_2)=\frac{\sigma_f^2}{4\pi}b_1b_2\exp\left[-\frac{1}{4}(b_1^2\kappa_1^2+b_2^2\kappa_2^2)\right] \tag{20}$$

where σ_f denotes the standard deviation of the stochastic field and b_1, b_2 denote the parameters that influence the shape of the spectrum which are proportional to the correlation distances of the stochastic field along the x_1, x_2 axes, respectively (Shinozuka and Deodatis 1996).

Using Eq. (8), a large number N_{SAMP} of sample functions are produced, leading to the generation of a set of stochastic stiffness matrices. The associated structural problem is solved N_{SAMP}

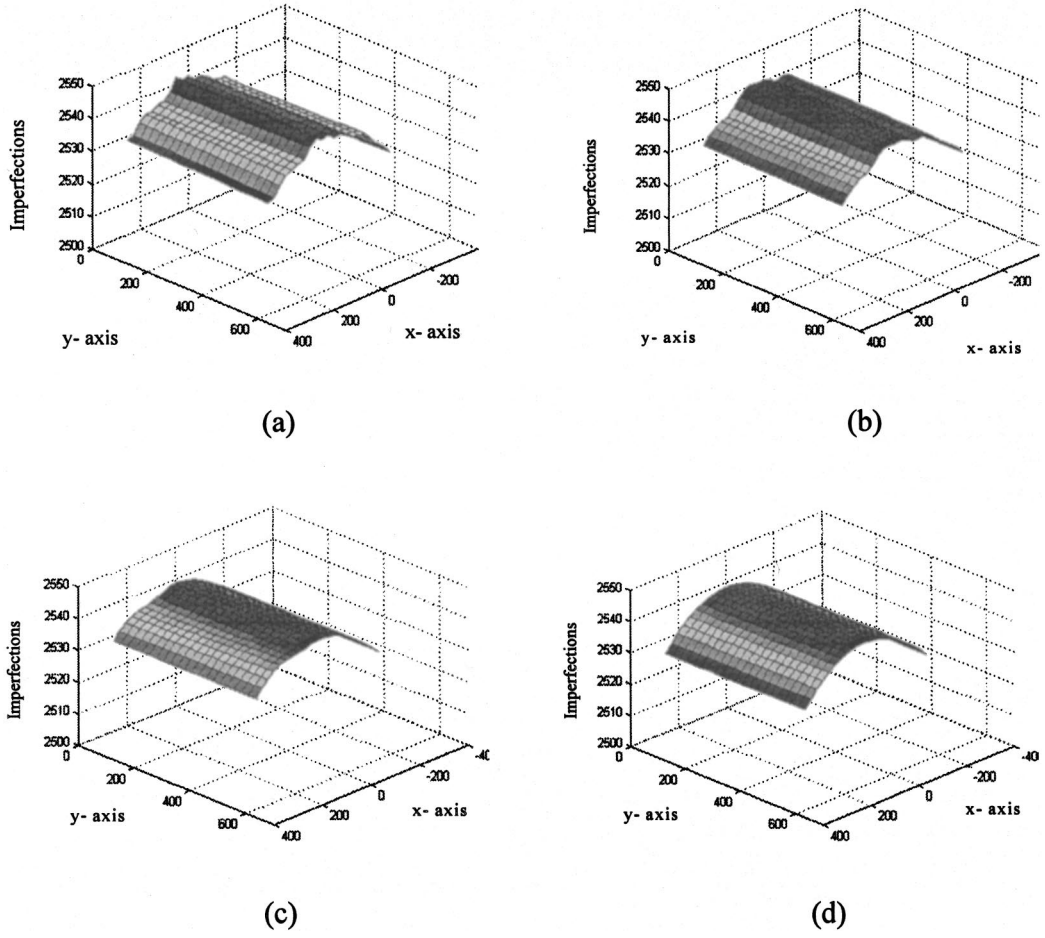

Fig. 5. One sample function of 1-D initial imperfection shapes of the cylindrical panel for $\sigma_f=0.10$ and for different correlation length parameters: (a) $b_1=25$ mm, (b) $b_1=50$ mm, (c) $b_1=100$ mm, and (d) $b_1=200$ mm

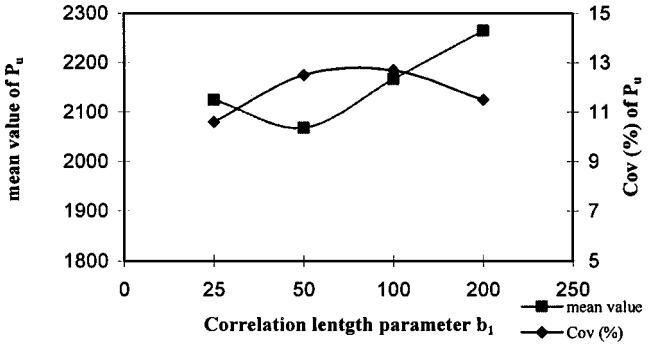

Fig. 6. Mean value and coefficient of variation (Cov%) of the ultimate load P_u as a function of the correlation length parameter b_1 for 1-D stochastic imperfections ($\sigma_f = 10\%$)

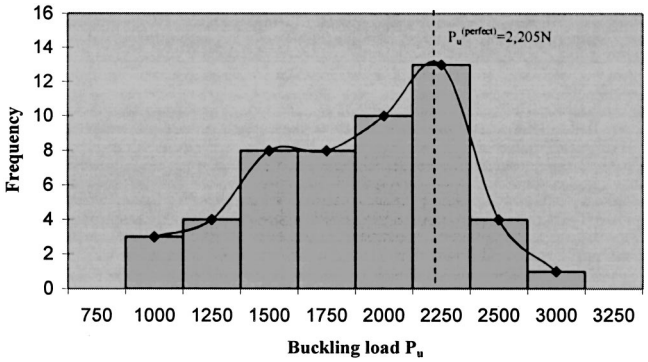

Fig. 8. Histogram of the critical load factor P_u for 1-D stochastic imperfections, $\sigma_f = 20\%$ and $b_1 = 50$ mm

times, while the response variability can finally be calculated by taking the response statistics of the N_{SAMP} simulations.

Numerical Examples

The hinged isotropic shallow cylindrical panel of Fig. 3 is selected as a testbed for the proposed methodology. This example, although not imperfection sensitive in the sense that it exhibits limit point instead of bifurcation buckling, is chosen because it is considered appropriate for the investigation of the sensitivity of the buckling load to initial imperfections in problems with a strongly nonlinear behavior. Loading as well as the geometric and material properties of the perfect shell are also shown in Fig. 3. The curve edge nodes of the panel are assumed to be free in all directions while the nodes along the sides are hinged (fixed against translation). The nonlinear displacement response of point *A* of the perfect cylinder with respect to the applied vertical load *P*, is shown in Fig. 4, where the cylindrical panel is discretized with a 16×16 mesh of TRIC shell elements. A mesh convergence study for this particular example is presented in a previous investigation (Argyris et al. 1988). In that investigation, it was also shown that a reduction of computing time by an order of magnitude was achieved for this particular example using the TRIC shell element compared to the computing time required by a typical 8-node serendipity shell element (Hinton and Owen 1984). This gives an indication of the computational efficiency of the TRIC element in nonlinear shell analysis. The same mesh size is used for the discretization of the stochastic fields since it is a fraction of the correlation length parameters used in the example and therefore, it is considered dense enough for the accurate representation of the fluctuations of the stochastic fields (Li and Der Kiureghian 1992). The ultimate load of the perfect configuration is found to be $P_u = 2{,}205$ N.

Initial Geometric Imperfections

Both one-dimensional (1-D) and 2-D stochastic imperfections are introduced to the model in order to investigate their effect on the buckling load of the panel. The thickness of the shell is considered to be equal to the height *h* at the apex, i.e., $t = 12.7$ mm. The 1-D stochastic imperfections are introduced in the free edge direction. The standard deviation σ_f of the stochastic field of the imperfections is assumed to be 10%. Four different values of the correlation length parameter b_1, which influences the shape of the power spectrum, are used. For each corresponding power spectrum, one full Monte Carlo simulation procedure is performed to obtain the variability of the critical load factor of the panel using a sample size $N_{\text{samp}} = 100$ which is considered sufficient for an accurate estimation of the mean value and the standard deviation of the buckling loads. In Fig. 5 one sample function for each correlation parameter b_1 is presented. In Fig. 6, the mean value and the coefficient of variation [Cov(%)] are plotted against the correlation length of the stochastic field. From this figure it can be seen that the ''worst'' imperfection mode related to the lowest mean value of buckling loads corresponds to a correlation length of $b_1 = 50$ mm, while the response variability is

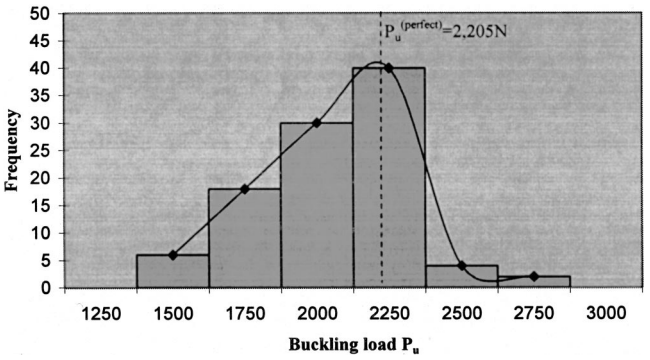

Fig. 7. Histogram of the critical load factor P_u for 1-D stochastic imperfections, $\sigma_f = 10\%$ and $b_1 = 50$ mm

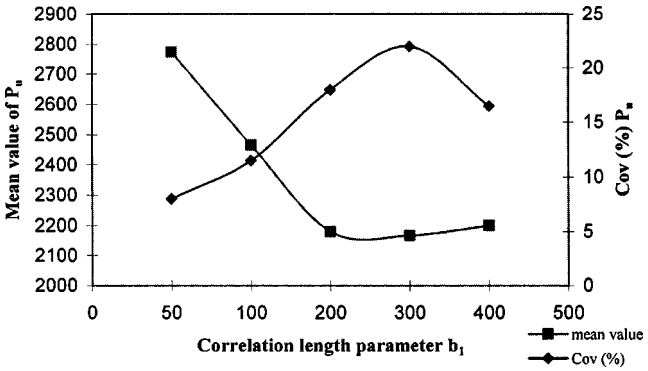

Fig. 9. Mean value and coefficient of variation (Cov%) of the ultimate load P_u as a function of the correlation length parameter b_1 for 2-D stochastic imperfections ($\sigma_f = 20\%$)

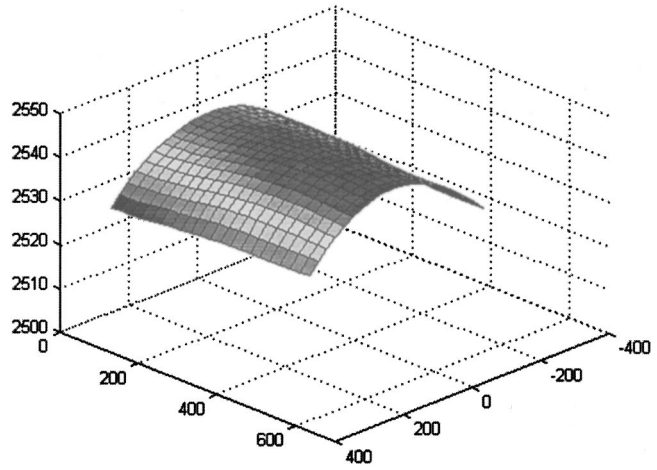

Fig. 10. 2-D initial imperfection shape for $\sigma_f = 0.20$ and correlation length parameter $b_1 = b_2 = 250$ mm

almost invariant for the examined correlation lengths and remains in the range of the corresponding input variability (10%). An additional MCS procedure with the same sample size is performed for $\sigma_f = 20\%$ and for the "worst" imperfection mode corresponding to $b_1 = 50$ mm. Figs. 7 and 8 present the histograms of the buckling loads for this value of the parameter b_1 for $\sigma_f = 10\%$ and $\sigma_f = 20\%$, respectively. The mean value of the buckling load is found to be 2,050 N for both cases, while a first estimate of the lowest buckling load is computed at 1,520 and 1,060 N for the two coefficients of variation, respectively.

The same steps are followed for the case of the 2-D stochastic imperfections. For this case, the value of the standard deviation is assumed to be $\sigma_f = 20\%$. In Fig. 9, the mean value and the coefficient of variation are plotted against the correlation length of the stochastic field. It is assumed that the correlation lengths in both x and y directions are equal, $b_1 = b_2$, since there are no specific manufacturing procedures or boundary conditions that would indicate a different assumption. From Fig. 9, a stiffening behavior of the panel for small values of the correlation length parameter b is observed. It is worth mentioning that this stiffening behavior was also observed by Deml and Wunderlich (1997) in shells with small slenderness and large imperfection amplitudes. It can also be seen that the "worst" imperfection mode corresponds to a correlation length of $b_1 = b_2 = 250$ mm as opposed to the correlation length of $b_1 = b_2 = 50$ mm for the 1-D case. Fig. 9 also reveals that the response variability is much more sensitive with regard to the correlation length parameters than the corresponding

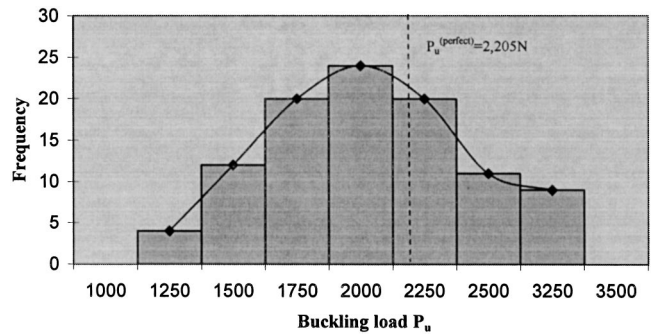

Fig. 11. Histogram of the critical load factor P_u for 2-D stochastic imperfections, $\sigma_f = 20\%$ and $b_1 = b_2 = 250$ mm

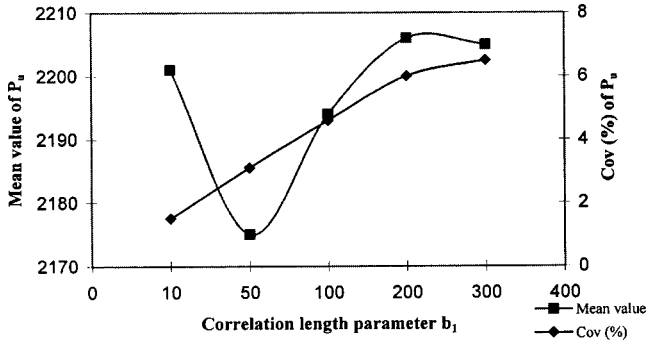

Fig. 12. Mean value and coefficient of variation (Cov%) of the ultimate load P_u as a function of the correlation length parameter b_1 for 1-D variation of the modulus of elasticity ($\sigma_f = 10\%$)

variability of the 1-D stochastic imperfections. Fig. 10 presents the shape of the "worst" imperfection mode obtained at $b_1 = b_2 = 250$ mm, while Fig. 11 depicts the histogram of the buckling loads for this mode of imperfections. The mean value of the buckling load is found to be 2170 N, while a first estimate of the lowest buckling load is found to be 1,250 N, which corresponds to a reduction of about 60% with respect to the buckling load of the perfect panel.

Material and Thickness Imperfections

Similar tests are performed for the investigation of the influence of material and thickness spatial variability on the buckling behavior of the panel. In Fig. 12, the mean value and the coefficient of variation are plotted against the correlation parameter b_1, for a 1-D stochastic variation of the Young modulus of the structure in the direction of the free edges, with $\sigma_f = 10\%$. The first estimate of the "worst" imperfection mode corresponds, as in the previous test case, to the correlation length parameter $b_1 = 50$ mm, while it can be seen that the coefficient of variation of the buckling load remains much smaller than the input coefficient of variation of the modulus of elasticity. The coefficient of variation tends to reach a plateau near σ_f for large correlation length parameters for which the modulus of elasticity becomes a single random variable. Similar results are obtained, as can be seen in Fig. 13, when a 1-D variation of the thickness is considered. The 2-D variation of the Young modulus and thickness is examined in Figs. 14 and 15 for

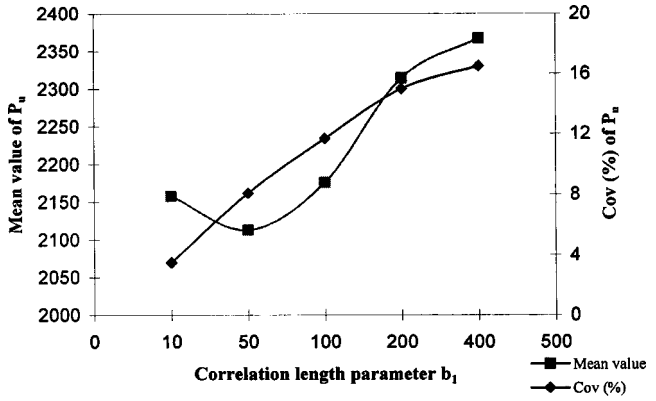

Fig. 13. Mean value and coefficient of variation (Cov%) of the ultimate load P_u as a function of the correlation length parameter b_1 for 1-D variation of the thickness ($\sigma_f = 10\%$)

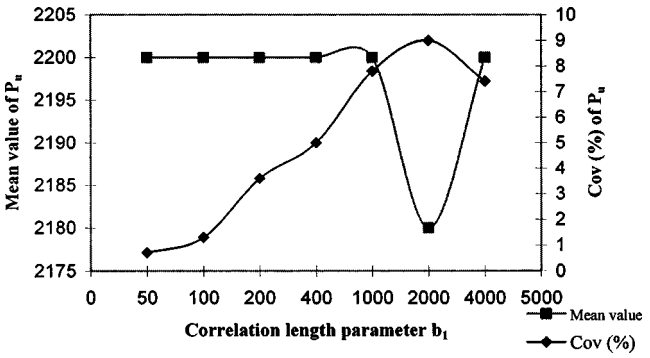

Fig. 14. Mean value and coefficient of variation (Cov%) of the ultimate load P_u as a function of the correlation length parameter b_1 for 2-D variation of the modulus of elasticity ($\sigma_f = 10\%$)

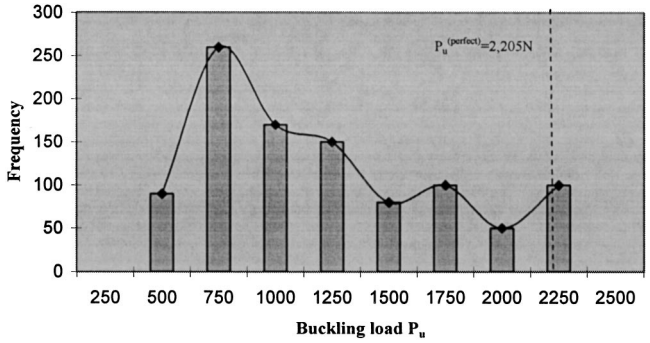

Fig. 16. Histogram of the critical load factor P_u for 1-D variation of combined geometrical, material and thickness imperfections ($\sigma_f = 20\%$)

$\sigma_f = 10\%$, respectively. From these figures it can be seen that the "worst" imperfection mode corresponds to a correlation parameter $b_1 = b_2 = 2{,}000$ mm which is markedly different than $b_1 = b_2 = 250$ mm which corresponds to the "worst" imperfection mode for initial geometric imperfections. Furthermore, the coefficient of variation of the buckling loads reaches a maximum value of around σ_f for the material imperfections, while the maximum covariance of the buckling loads reaches 17% for the 2-D variation of thickness. The mean value of the buckling load for both material and thickness variation is found to be almost the same with the buckling load of the perfect shell.

Combined Geometrical, Material, and Thickness Imperfections

All the above imperfections are now combined and introduced simultaneously to the model. For this purpose the "worst" imperfection modes and the corresponding correlation length parameters are depicted from the previously studied cases. For a 1-D combined variation of stochastic imperfections the value of $b_1 = 50$ mm is considered for all parameters with a standard deviation of $\sigma_f = 20\%$. For the combined imperfections all Monte Carlo simulations are performed using a sample size $N_{\text{samp}} = 1{,}000$, as opposed to $N_{\text{samp}} = 100$ used in the previous cases, since a larger sample size is required for the accurate prediction of the "exact" lowest buckling load of the panel. Fig. 16 presents the histogram of the buckling loads for this case. From a comparison of this figure and Fig. 8, the quantitative as well as the qualitative difference of the buckling loads distribution can be observed with respect to the stand alone imperfection cases. The drastic reduction in the buckling load values as well as the larger scatter of the results for the combined imperfection cases can be observed. The mean value of the buckling loads for this simulation is found to be $\bar{P}_u = 1{,}228$ N which amounts to about half of the buckling load of the perfect structure. The coefficient of variation of P_u is found to be 45%, which is more than double the coefficient of variation of the uncertain parameters, while the lowest buckling load in this simulation is found to be $P_u = 525$ N corresponding to the 25% of the buckling load of the perfect structure.

For the 2-D variation of combined imperfections, the values $b_1 = b_2 = 300$ mm are considered for the stochastic field describing the initial geometric imperfections and $b_1 = b_2 = 2{,}000$ mm for the modulus of elasticity and the thickness of the shell. All parameters are assumed to have a standard deviation of $\sigma_f = 20\%$. Fig. 17 presents the histogram of the buckling loads for this case study. From this figure it can be seen that the scatter of the buckling loads is more pronounced than the 1-D variation depicted in Fig. 16. The mean value of the buckling loads for this case is found to be $\bar{P}_u = 2{,}250$ N, which is almost the same as the buckling load of the perfect structure. The coefficient of variation of P_u, on the other hand, is found to be 50%, which corresponds to more than twice the value of coefficient of variation of the uncertain parameters. Furthermore, the lowest buckling load in this simulation is found to be $P_u = 300$ N, which reaches the 15% of the buckling load of the perfect structure.

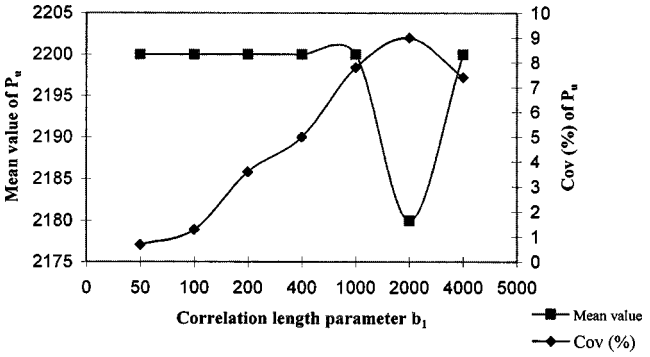

Fig. 15. Mean value and coefficient of variation (Cov%) of the ultimate load P_u as a function of the correlation length parameter b_1 for 2-D variation of the thickness ($\sigma_f = 10\%$)

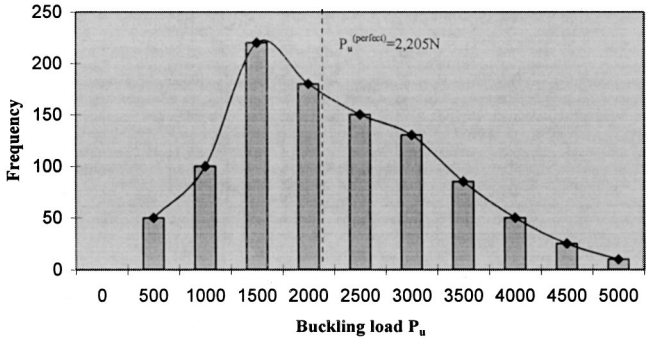

Fig. 17. Histogram of the critical load factor P_u for 2-D variation of combined geometrical, material and thickness imperfections ($\sigma_f = 20\%$)

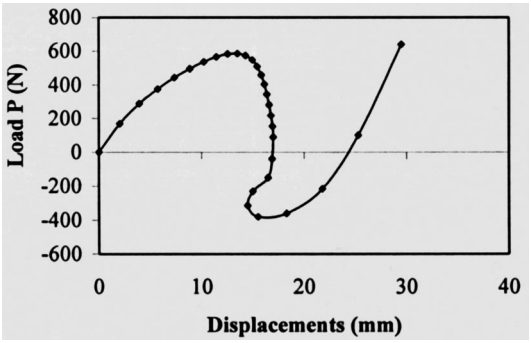

Fig. 18. Central load—displacement curve of the perfect cylindrical panel ($t=6.35$ mm)

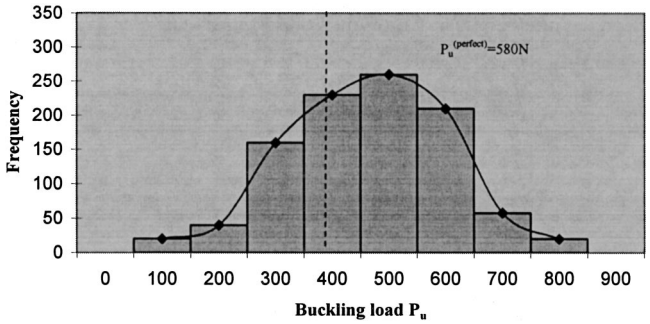

Fig. 20. Histogram of the critical load factor P_u for 2-D variation of combined geometrical, material, and thickness imperfections ($\sigma_f=20\%$)

The previous investigation for the combined imperfections are repeated for the same cylindrical panel of Fig. 3 but with half its thickness, i.e., $t=6.35$ mm. The nonlinear response of point A of the perfect cylinder with respect to the applied vertical load P, is shown in Fig. 18. From the load-displacement curve it can be seen that this shell structure exhibits a higher degree of sensitivity to the deformed geometry than the previous thicker shell structure. The ultimate load of the perfect configuration is found to be $P_u=580$ N. Fig. 19 presents the histogram of the buckling loads for the case of 1-D variation of the combined imperfections. It can be seen that the significant reduction observed for the mean value of the buckling loads, with respect to the buckling load of the perfect shell, as well as the scatter of the buckling loads, are more or less similar to the reduction and scatter observed for the thicker shell. More specifically, the mean value of the buckling loads for this case is found to be $\overline{P}_u=360$ N and the coefficient of variation of P_u is 45%. The lowest buckling load in this case is found to be $P_u=120$ N, which is 20% of the buckling load of the perfect structure.

Fig. 20 presents the histogram of the buckling loads for the case of 2-D variation of the combined imperfections for the thinner cylinder. This histogram gives a distribution of the buckling loads somewhat different than the corresponding distribution of the thicker shell as can be seen in Fig. 17. A small reduction is observed in the mean value of the buckling loads with respect to the buckling load of the perfect shell ($\overline{P}_u=480$ N compared to $P_u=580$ N), while the scatter of the buckling loads is not as wide as the scatter observed in the thicker shell (coefficient of variation 30% of $\overline{P}_u$). The lowest buckling load in this case is found to be $P_u=120$ N, which is 20% of the buckling load of the perfect structure.

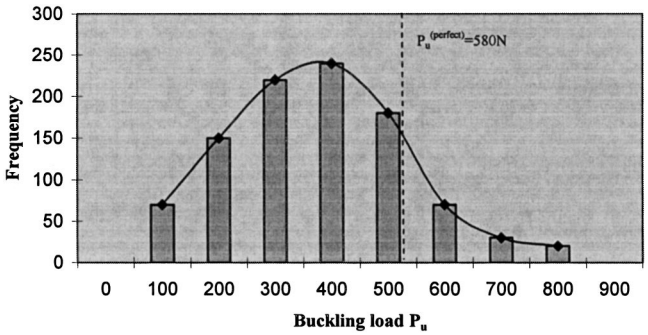

Fig. 19. Histogram of the critical load factor P_u for 1-D variation of combined geometrical, material and thickness imperfections ($\sigma_f=20\%$)

Conclusions

In this paper, a methodology is presented for the stochastic finite-element analysis of shells which takes into consideration stability aspects of shells with combined random initial geometric imperfections, material properties, as well as shell thickness. The accurate representation of these imperfections using the stochastic field theory in the context of a Monte Carlo simulation procedure, in conjunction with a robust and computationally efficient nonlinear finite-element formulation with the TRIC shell element, allows for an accurate and cost effective prediction of the large scatter of the buckling load of any type of shell structure. This scatter has repetitively been observed in relative experiments.

Using the proposed methodology, a parametric study is performed for the evaluation of the sensitivity of the buckling load of a cylindrical panel to the amplitude and shape of the imperfections. In particular, both 1-D and 2-D stochastic imperfections are introduced for all stochastic parameters (i.e., shape imperfections, modulus of elasticity, and shell thickness) as stand alone or combined cases. For all cases the influence of the shape and magnitude of the imperfections to the shape and magnitude of the distribution of the buckling loads of the panel is investigated.

This investigation revealed some very interesting aspects for the buckling behavior of cylindrical panels in the presence of combined random initial imperfections. More specifically, for the case of 1-D combined imperfections a drastic reduction of about 50% in the mean value of the buckling load is observed accompanied by a twofold increase of the coefficient of variation, compared to a marginal reduction for the stand-alone case of 1-D initial geometric imperfections. For 2-D combined imperfections, however, the observed twofold increase of the coefficient of variation of the buckling loads was not followed by a similar decrease of the mean value which remained the same and almost equal to the buckling load of the perfect shell. In addition the computed response of the thinner shell revealed that for 1-D combined imperfections, the distribution of the buckling loads preserves its characteristics compared to the thicker shell. Furthermore, for 2-D combined imperfections, the increase of sensitivity of the thinner shell to the deformed geometry resulted in a substantial decrease of the sensitivity of the shell to the variability of initial imperfecions.

Using this procedure it can be made possible not only to efficiently and accurately predict the large scatter of the buckling loads of any type of real world shell structure but also to estimate the ''worst'' imperfection shape and the corresponding ''exact'' lower bound of the buckling load. The latest information is most valuable for the safe design of shells against buckling. However, general conclusions about the buckling behavior of shells in the presence of initial imperfections cannot be deduced from the presented numerical results since any generalization would require a variety of examples to be tested. The application of the presented methodology in a variety of test examples including realistic structures with many degrees of freedom as well as realistic assumptions concerning the nonhomogeneity of the random fields will be the subject of future research.

References

Albertin, U., and Wunderlich, W. (2000). ''Buckling design of imperfect spherical shells.'' *Proc., 4th Int. Colloquium on Computation of Shell and Spatial Structures*, M. Papadrakakis, A. Samartin, and E. Onate, eds., IASS-IACM 2000, Chania—Crete, Greece.

Argyris, J. H., Papadrakakis, M., Apostolopoulou, C., and Koutsourelakis, S. (2000). ''The TRIC shell element: Theoretical and numerical inverstigation.'' *Comput. Methods Appl. Mech. Eng.*, 182, 217–245.

Argyris, J. H., Papadrakakis, M., and Stefanou, G. (2002). ''Stochastic finite element analysis of shells.'' *Comput. Methods Appl. Mech. Eng.*, 191, 4781–4804.

Argyris, J. H., Tenek, L., and Olofsson, L. (1997). ''*TRIC*, a simple but sophisticated 3node triangular element based on 6 rigid-body and 12 straining modes for fast computational simulations of arbitrary isotropic and laminated composite shells.'' *Comput. Methods Appl. Mech. Eng.*, 145, 11–85.

Argyris, J. H., Tenek, L., Papadrakakis, M., and Apostolopoulou, C. (1998). ''Postbuckling performance of the TRIC natural mode triangular element for isotropic and laminated composite shells.'' *Comput. Methods Appl. Mech. Eng.*, 166, 211–231.

Chryssanthopoulos, M. K., and Poggi, C. (1995). ''Probabilistic imperfection sensitivity analysis of axially compressed composite cylinders.'' *Eng. Struct.*, 17, 398–406.

Deml, M., and Wunderlich, W. (1997). ''Direct evaluation of the 'worst' imperfection shape in shell buckling.'' *Comput. Methods Appl. Mech. Eng.*, 149, 201–222.

Elishakoff, I., Li, Y. W., and Starnes, J. H., Jr. (1996). ''Imperfection sensitivity due to the elastic moduli in the Rooda-Koiter frame.'' *Chaos, Solitons Fractals*, 7, 1179–1186.

Hinton, E., and Owen, D. R. J. (1984). *Finite element software for plates and shells*, Pineridge, Swansea, U.K., 1984.

Koiter, W. T., Elishakoff, I., Li, Y. W., and Starnes, J. H., Jr. (1994). ''Buckling analysis of an axially compressed cylindrical shell under axial compression.'' *Int. J. Solids Struct.*, 31, 795–805.

Li, C.-C., and Der Kiureghian, A. (1992). ''An optimal discretization of random fields.'' *Technical Rep. UCB/SEMM-92/04*, Department of Civil Engineering, University of Berkeley, Calif.

Li, Y. W., Elishakoff, I., Starnes, J. H., Jr., and Bushnell, D. (1997). ''Effect of the thickness variation and initial imperfection on buckling of composite shells: Asymptotic analysis and numerical results by BOSOR4 and PANDA2.'' *Int. J. Solids Struct.*, 34, 3755–3767.

Popescu, R., Deodatis, G., and Prevost, J. H. (1998). ''Simulation of homogeneous nonGaussian stochastic vector fields.'' *Probab. Eng. Mech.*, 13, 1–13.

Schenk, C. A., Schueller, G. I., and Arbocz, J. (2000). ''On the analysis of cylindrical shells with random imperfections.'' *Proc., 4th Int. Colloquium on Computation of Shell and Spatial Structures*, M. Papadrakakis, A. Samartin, and E. Onate, eds., IASS-IACM 2000, Chania—Crete, Greece.

Shinozuka, M., and Deodatis, G. (1996). ''Simulation of multidimensional Gaussian stochastic fields by spectral representation.'' *Appl. Mech. Rev.*, 49, 29–53.

Vanmarcke, E. (1983). *Random fields: Analysis and synthesis*, MIT, Cambridge, Mass.